© 2014. Published by The Company of Biologists Ltd | Development (2014) 141, 2225-2234 doi:10.1242/dev.105817

RESEARCH ARTICLE

STEM CELLS AND REGENERATION

Mature osteoblasts dedifferentiate in response to traumatic bone injury in the zebrafish fin and skull

Karina Geurtzen[1,*], Franziska Knopf[1,2,*], Daniel Wehner[3], Leonie F. A. Huitema[4], Stefan Schulte-Merker[4,5,6] and Gilbert Weidinger[3,‡]

ABSTRACT

Zebrafish have an unlimited capacity to regenerate bone after fin amputation. In this process, mature osteoblasts dedifferentiate to osteogenic precursor cells and thus represent an important source of newly forming bone. By contrast, differentiated osteoblasts do not appear to contribute to repair of bone injuries in mammals; rather, osteoblasts form anew from mesenchymal stem cells. This raises the question whether osteoblast dedifferentiation is specific to appendage regeneration, a special feature of the lepidotrichia bone of the fish fin, or a process found more generally in fish bone. Here, we show that dedifferentiation of mature osteoblasts is not restricted to fin regeneration after amputation, but also occurs during repair of zebrafish fin fractures and skull injuries. In both models, mature osteoblasts surrounding the injury downregulate the expression of differentiation markers, upregulate markers of the pre-osteoblast state and become proliferative. Making use of photoconvertible Kaede protein as well as Cre-driven genetic fate mapping, we show that osteoblasts migrate to the site of injury to replace damaged tissue. Our findings suggest a fundamental role for osteoblast dedifferentiation in reparative bone formation in fish and indicate that adult fish osteoblasts display elevated cellular plasticity compared with mammalian bone-forming cells.

KEY WORDS: Dedifferentiation, Osteoblast, Bone, Fracture, Injury, Zebrafish, Lepidotrichia, Skull, Osteocalcin, Kaede

INTRODUCTION

In contrast to mammals, adult fish and urodele amphibia (salamanders and newts) can efficiently regenerate appendages (fins and limbs) after amputation. Bone is a major element of appendages, and the ability to regenerate bony structures during fin and limb regeneration appears to be essentially unlimited (Hall, 2005; Han et al., 2005). Bone repair also occurs in adult mammals, but internal bone defects can only be healed below a critical size (Hall, 2005), and regeneration of bony elements lost due to amputation does not occur. Interestingly, even in salamander limbs the capacity to regenerate bone after amputation is higher than the ability to repair internal bone defects, which – similar to mammals – can only be repaired below a critical size (Satoh et al., 2010). Intriguingly, transplantation of blastemal cells, undifferentiated progenitors that form after limb amputation, into a critical size bone defect can rescue repair of such bone injuries (Satoh et al., 2010). Thus, it is conceivable that different cellular mechanisms underlie bone defect repair and bone regeneration in the context of an amputated appendage.

Identification of the cellular source of regenerating appendages has been a long-standing issue in regeneration research. Although many adult tissues contain stem cells, whose activation and expansion could drive regeneration, adult differentiated cells can also represent sources of newly forming tissue (Tanaka and Reddien, 2011). Indeed, we and others have recently discovered that mature osteoblasts dedifferentiate to lineage-restricted osteoblast progenitors and thus provide an important source of newly forming bone during regeneration of the zebrafish caudal fin (Knopf et al., 2011; Sousa et al., 2011). Dedifferentiation, 'a process in which a cell loses its specialized morphology, function and biochemistry to initiate cell division and reverts to a less differentiated state in order to redifferentiate again' (Hall, 2005), is generally assumed to occur during salamander and teleost fish appendage regeneration (Monaghan and Maden, 2013). Recently, genetic lineage-tracing techniques have indeed shown that muscle regenerates from dedifferentiating muscle fibers in regenerating limbs of newts, but surprisingly not in axolotls, indicating that the cellular mechanisms of regeneration are diverse even within fairly closely related animal groups (Sandoval-Guzman et al., 2014).

Intriguingly, genetic lineage tracing has shown that mature osteoblasts do not contribute to bone repair in mammals (Park et al., 2012), and dedifferentiation of mature osteoblasts is not considered to occur in mammalian bone biology [with the possible exception of pediatric osteosarcomas (Pereira et al., 2009)]. Instead, during mammalian fracture healing, new osteoblasts appear to be supplied from mesenchymal stem cells, which, however, are restricted to only give rise to osteoblasts *in vivo* (Park et al., 2012). Thus, mature differentiated cells represent an important source of regenerating bone in adult fish, but not during fracture repair in mammals.

This raises the following possibilities: (1) osteoblast dedifferentiation is associated with appendage regeneration (which does not happen in mammals), but does not occur during bone repair (which is common to fish and mammals); (2) it only occurs in the bones of the fish fin (the lepidotrichia), which have been suggested to represent a distinct type of skeletal tissue not found in mammals based on their extracellular matrix composition (Marí-Beffa et al., 2007); or (3) teleost bone-forming cells are more plastic than mammalian osteoblasts, and their dedifferentiation is an important feature during fin regeneration and repair of internal bone defects in all teleost bones.

Here, by introducing injuries in bone tissue of the zebrafish fin and skull, we have addressed these questions and found that osteoblast dedifferentiation in teleosts does not only operate during appendage regeneration, but also during repair processes caused by other types of injury.

[1]Biotechnology Center and CRTD, Technische Universität Dresden, 01307 Dresden, Germany. [2]Kennedy Institute of Rheumatology, Oxford OX3 7FY, UK. [3]Institute for Biochemistry and Molecular Biology, Ulm University, 89081 Ulm, Germany. [4]Hubrecht Institut-KNAW & UMC Utrecht, 3584 CT Utrecht, The Netherlands. [5]EZO, WUR, 6709 PG Wageningen, The Netherlands. [6]Institute of Cardiovascular Organogenesis and Regeneration, University of Münster, 48149 Münster, Germany.
*These authors contributed equally to this work

‡Author for correspondence (gilbert.weidinger@uni-ulm.de)

Received 8 November 2013; Accepted 9 April 2014

Development (2014) 141, 2225-2234 doi:10.1242/dev.105817

RESULTS

Fin ray fractures – a new model of bone repair

To test whether osteoblast dedifferentiation is a process specific to appendage regeneration or whether mature osteoblasts are also involved in repair of more limited bone injuries, we induced fractures in the intramembranous bony fin rays of the zebrafish caudal fin. Fin rays contain segmented dermal bones (lepidotrichia) composed of two concave hemirays facing each other. These hemirays enclose fibroblasts, blood vessels, nerves and pigment cells and are covered by epidermis. A single layer of osteoblasts lines the bone matrix on the in- and outside of the hemirays (Knopf et al., 2011). By applying mechanical force, we induced distinct transverse cracks within a single segment of the bony rays, which typically affected only one of the two hemirays. These fractures differ from a recently developed crush injury model, in which several bone fragments were produced at the site of damage, in addition to the actual fracture crack (Sousa et al., 2012). We did not stabilize these fractures and assayed the repair process by repeated imaging over a period of several weeks. At 1 day post injury (dpi) and 2 dpi we observed a thickening of the tissue at the fracture site (Fig. 1A, arrow; supplementary material Fig. S1A, asterisk; see Table S1 for experimental numbers), which mostly represented epidermal tissue, as in *keratin4*:AmCyan transgenic fish, an epidermal reporter line (Wehner et al., 2014), *keratin4* promoter activity could be detected in most of the cells of this swelling (Fig. 1B). In contrast to crush-injured fins (Sousa et al., 2012), the thickened epidermis was restricted to the fractured segment, illustrating different fracture severities. At 6-7 dpi, a thickening had formed that consisted of collagen fibers, as indicated by blue staining with Acid Fuchsin Orange G (AFOG) and Toluidine Blue (Fig. 1A,C; supplementary material Fig. S1B) (Constantine and Mowry, 1968). This 'hard callus' also stained positive for Alizarin Red and Calcein and thus represented calcifying bone matrix (Fig. 1D,E). Osteoblasts staining positive for the pan-osteoblast antigen Zns5 (Johnson and Weston, 1995) lined the callus matrix, which, however, at 6 dpi did not contain Osteocalcin protein, indicating that the tissue had not yet transformed to mature bone tissue (Fig. 1F), in contrast to 28 dpi, when Osteocalcin protein was detected in the callus (Fig. 1G). At 4 weeks post injury, the fracture crack was not visible in whole-mount views of fractured fin rays any longer (Fig. 1A). However, longitudinal sections revealed that the old bone was still distinguishable from the surrounding new bone matrix and still contained a crack (Fig. 1H). Injured segments displayed a thickened appearance (Fig. 1A, arrowhead) even at 17 weeks and 1 year post injury (supplementary material Fig. S1C,D). We conclude that non-stabilized fractures to lepidotrichia bone are repaired by deposition of new bone matrix, but that the old bone of the fracture itself does not

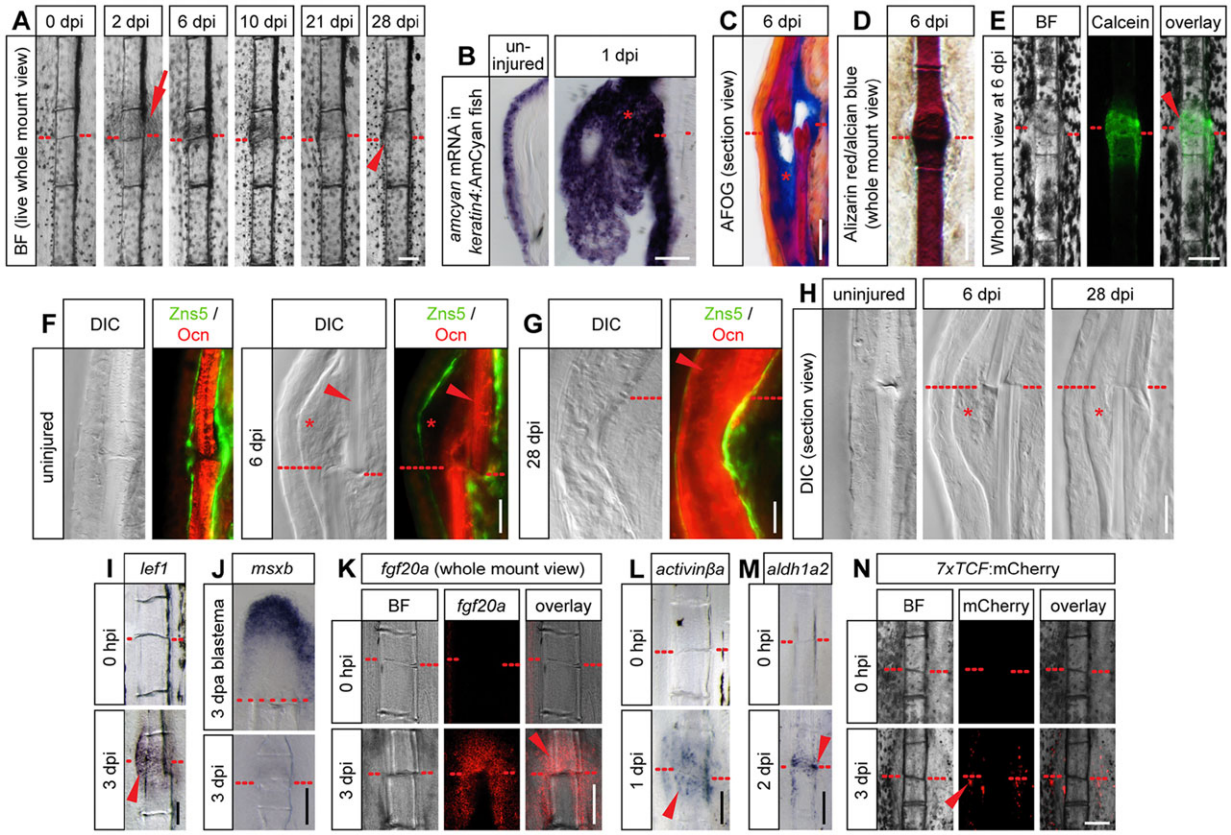

Fig. 1. Fracture model in zebrafish bony fin rays. (A) Whole-mount view of the same fractured fin ray at different time points post injury. Red dashed line, fracture; arrow, epidermal thickening; arrowhead, thickened bone. (B) Epidermal thickening at 1 dpi identified by *in situ* hybridization against *amcyan* mRNA in *keratin4*:AmCyan transgenic fish. (C) Longitudinal section view of an AFOG-stained fin hemiray at 6 dpi with collagen staining blue (asterisk). (D) Whole-mount view of an Alizarin Red/Alcian Blue stained fin ray at 6 dpi. The lack of blue staining indicates intramembranous ossification. (E) Whole-mount view of a fin ray at 6 dpi stained with Calcein indicates calcium incorporation into the mineralizing callus. (F,G) Immunofluorescence on longitudinal sections of individual hemirays stained for the pan-osteoblast marker Zns5 and Osteocalcin (Ocn), labeling mature bone matrix. Note the absence of Osteocalcin in the callus tissue at 6 dpi (asterisk), but presence at 28 dpi (arrowhead). DIC, differential interference contrast. (H) Longitudinal sections of individual fractured hemirays. Asterisk, hard callus. (I-M) Expression of the indicated genes detected by chromogenic (I,J,L,M) or fluorescent (K) whole-mount *in situ* hybridizations on fractured rays or amputated fins (J). (N) mCherry fluorescence is induced in fractured *7xTCF*:mCherry Wnt reporter fish at 3 dpi. Scale bars: 100 µm in A,D,E,I-N; 50 µm in B,C; 20 µm in F-H. BF, brightfield.

Development (2014) 141, 2225-2234 doi:10.1242/dev.105817

reunite. Furthermore, remodeling processes that would restore the original bone morphology appear to be slow, similar to those observed in human fracture repair, where remodeling continues up to several years after a fracture (Cameron et al., 2013).

We next asked whether lepidotrichia fractures induce a similar molecular response to fin amputation. During regeneration after amputation a multilayered wound epidermis forms, which surrounds the blastema, a population of proliferative, lineage-restricted progenitor cells characteristic to regenerating appendages (Lee et al., 2009; Monaghan and Maden, 2013). *lef1* marks a subregion of the wound epidermis (Poss et al., 2000a), and robust *lef1* expression was also induced in tissue surrounding fractures at 3 dpi (Fig. 1I). By contrast, while we could readily detect expression of the regeneration blastema marker *msxb* after amputation, expression at fractures was neither detected by whole mount *in situ* hybridization (Fig. 1J) nor qRT-PCR (data not shown), which differs from previously reported results using more severe crush injuries (Sousa et al., 2012). However, signaling pathways known to be required for fin regeneration appear to be activated in response to fractures as well. In particular, we detected expression of *fgf20a* (Fig. 1K), *activinβa* (*inhbaa* – ZFIN) (Fig. 1L), *aldh1a2* (*raldh2*, the rate-limiting enzyme in retinoic acid synthesis; Fig. 1M) and activity of Wnt/β-catenin signaling as reported by the *7xTCF-Xla.Siam*:nlsmCherry^{la5} (*7xTCF*:mCherry) transgenic line (Moro et al., 2012) (Fig. 1N). This indicates that repair of fin ray fractures requires a similar signaling environment to regeneration after amputation, despite the lack of *msxb* expression. Notably, FGF, Wnt, RA and Activin pathway components all have been shown to be involved in mammalian bone homeostasis or repair (Nagamine et al., 1998; Barnes et al., 1999; Schmid et al., 2009; Komatsu et al., 2010; Conaway et al., 2013), illustrating their relevance both in mammalian and zebrafish fracture repair.

Osteoblasts dedifferentiate in response to fin ray fractures

We next asked whether mature osteoblasts dedifferentiate in response to lepidotrichia fracture. Osteocalcin is specifically expressed in differentiated osteoblasts, and *osteocalcin*:GFP transgenic fish can be used to label mature osteoblasts *in vivo* (Gavaia et al., 2006; Knopf et al., 2011). In the adult caudal fin, GFP fluorescence was found in the center of every fin ray segment, but was absent from the segment boundaries (Fig. 2A). In response to fracture, reporter fluorescence was progressively lost in the injured segment starting at 1 dpi (arrow in Fig. 2A; see quantification in supplementary material Fig. S2A), as well as in the segments directly neighboring the fractured segment starting at 2 dpi (arrowheads in Fig. 2A, quantification in Fig. 2B; supplementary material Fig. S2A). Thus, downregulation of reporter expression is observed in segments not directly affected by the injury. By contrast, reporter activity was neither significantly reduced in other segments of the injured fin ray nor in uninjured fin rays of the same fin, indicating that the response is not systemic (Fig. 2B; supplementary material Fig. S2A,B). qRT-PCR on RNA isolated from injured plus adjacent segments showed that endogenous *osteocalcin* expression was also reduced in response to fracture (Fig. 2C).

We next asked whether *osteocalcin*:GFP levels dropped as a result of loss of osteoblasts. Cells that failed to express *osteocalcin*:GFP in the vicinity of the fracture continued to express Zns5 (Fig. 2D), and their number did not significantly differ from that in uninjured fins (supplementary material Fig. S2C). Furthermore, although the number of apoptotic cells in the epidermis covering the fractured bone was significantly increased in the injured and directly adjacent segments, this was not the case in the fibroblast and osteoblast populations (Fig. 2E,F). Moreover, necrotic cells were mainly detected in epidermal tissue but not in the osteoblast layer (supplementary material Fig. S2D-F). Together, these data indicate that mature osteoblasts do not undergo enhanced cell death but downregulate *osteocalcin* expression in a distance up to roughly 500 µm from a bone fracture.

Next, we tested whether fractures also resulted in upregulation of pre-osteoblast markers. Expression of a *runx2:GFP* reporter was present at very low levels in osteoblasts of the adult fin, except for a small population of cells at the growing tip of each fin ray (Fig. 2G). After fracture, *runx2b* expression could be detected in the bone surrounding the fracture, as shown by whole-mount *in situ* hybridization against *gfp* RNA in *runx2:GFP* transgenic fish (Fig. 2H), as well as by qRT-PCR against endogenous *runx2b* (Fig. 2I). We additionally found Tenascin C, which is expressed in mesenchymal condensations prefiguring osteoblasts during development, and represents an indicator of cell migration and tissue rearrangement (Chiquet-Ehrismann and Tucker, 2004), to be induced in fibroblasts and osteoblasts after fracture (Fig. 2J,K). Together, these results indicate that mature osteoblasts in the zebrafish fin ray adopt the gene expression characteristics of pre-osteoblasts following bone fracture.

In contrast to postproliferative, *osteocalcin*+ osteoblasts, pre-osteoblasts are cycling cells. We thus checked whether osteoblasts would start to proliferate in response to fracture. Although hardly any osteoblasts went through S-phase of the cell cycle in uninjured fins, the number of BrdU-incorporating osteoblasts rose to 20% in the injured segment, and enhanced proliferation was induced up to at least 500 µm from the fracture site, thus also in adjacent bony segments (Fig. 2L,M). It is noteworthy that incorporation of BrdU indicating S-phase reentry was already significantly elevated in dedifferentiating osteoblasts at 1 dpi, contrasting with the observation that induction of proliferation was delayed during fracture repair after crush injury (Sousa et al., 2012).

Osteoblasts in the stump of the amputated fin change their morphology in the process of dedifferentiation (Knopf et al., 2011). To test whether this is also the case after fracture we performed transmission electron microscopy (TEM) on fractured fin rays. At 1 dpi, bone-lining osteoblasts had not considerably altered their morphology in comparison to uninjured fin ray osteoblasts (Fig. 2N; data not shown). By contrast, at 6 dpi osteoblasts displayed a less elongated nucleus and overall a more rounded shape (Fig. 2N). The cells had also formed prominent extracellular matrix, which is suggestive of a secretory cell status (ECM in Fig. 2N). Notably, at 4 weeks post injury, osteoblasts still showed a rounded secretory morphology (supplementary material Fig. S2G), whereas later, at 8 weeks post injury, cells had again adopted their pre-injury morphology, characterized by a highly elongated nucleus (supplementary material Fig. S2G).

Altogether, these results indicate that osteoblasts respond to fin ray fracture by downregulation of late and induction of early osteogenic genes, by re-entry into the cell cycle and by loss of their specialized morphology. Thus, mature osteoblasts dedifferentiate in fractured fins as they do in response to amputation (Knopf et al., 2011).

Osteoblasts actively migrate to the site of injury

We have recently provided evidence based on lineage tracing that dedifferentiated osteoblasts move toward the amputation plane in response to fin amputation (Knopf et al., 2011). As expression of Tenascin C, which has anti-adhesive properties, was induced after fin ray fracture, we asked whether osteoblasts migrate toward a fracture as well. To test this we made use of a transgenic line expressing the photoconvertible protein Kaede under control of

Development (2014) 141, 2225-2234 doi:10.1242/dev.105817

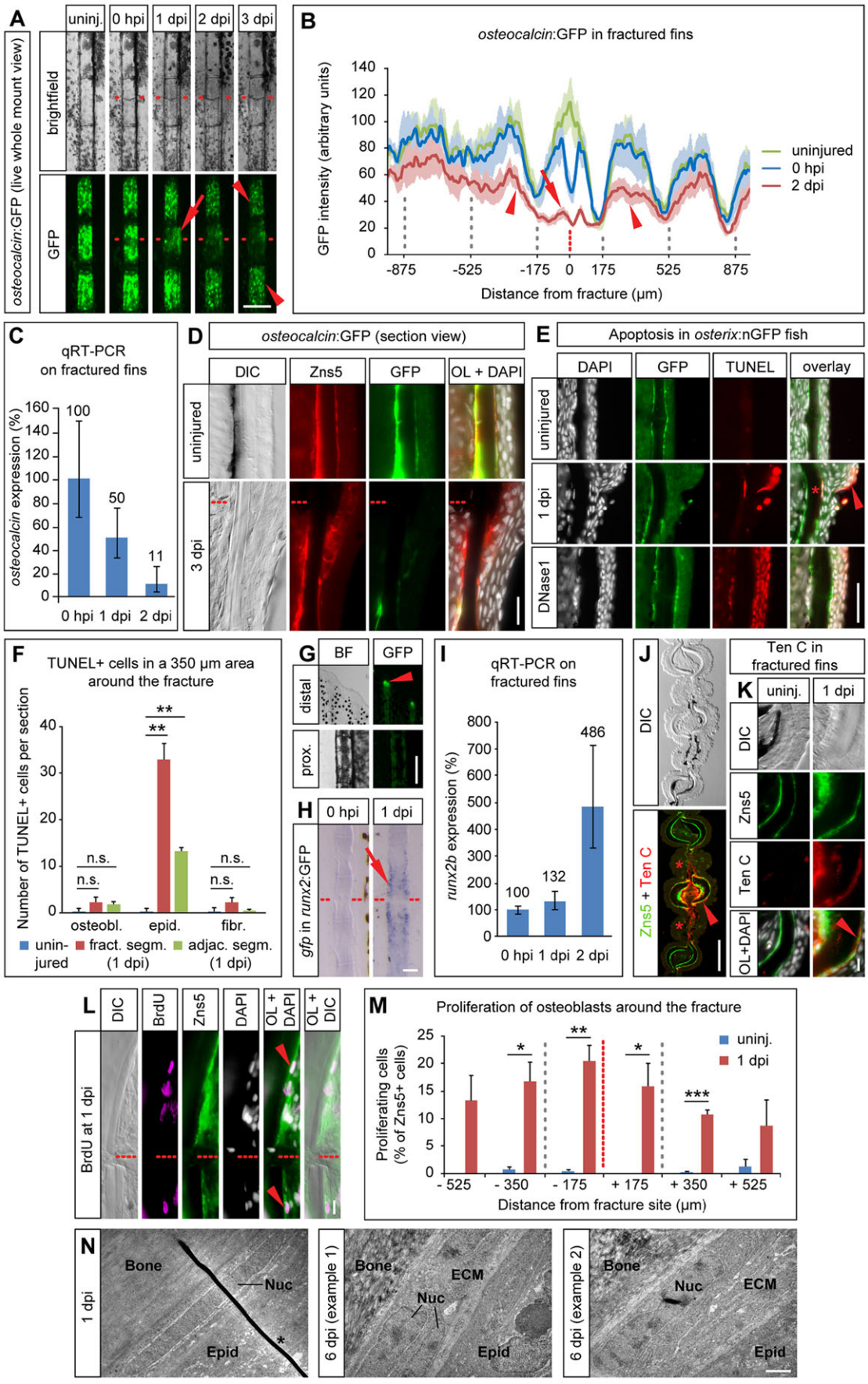

Fig. 2. See next page for legend.

Development (2014) 141, 2225-2234 doi:10.1242/dev.105817

Fig. 2. Osteoblasts in the fractured bony fin ray undergo dedifferentiation. (A) Live whole-mount view of a fractured fin ray in the same *osteocalcin*:GFP transgenic fish imaged at different time points. GFP levels drop in the fractured (arrow) and adjacent (arrowheads) segments. (B) Quantification of *osteocalcin*:GFP expression showing average GFP intensity±s.e.m. Arrow, fractured segment; arrowheads, adjacent segments. GFP intensity is not reduced by introduction of the fracture, except at the direct fracture site (compare blue curve with green curve). Gray dashed lines, segment boundaries. (C) Endogenous *osteocalcin* levels determined by qRT-PCR on fractured plus adjacent segments and shown relative to the levels at 0 hpi. Error bars, s.d. (D) Longitudinal section view of *osteocalcin*:GFP uninjured and 3 dpi hemirays stained with antibodies against GFP and Zns5. In contrast to uninjured fins, at 3 dpi GFP can be hardly detected in Zns5+ osteoblasts. OL, overlay. (E) Apoptotic cells detected by TUNEL staining in longitudinal sections of *osterix*:nGFP fish are mainly found in the epidermal cell layer overlying the fracture (arrowhead) and only occasionally in osteoblasts (asterisk). DNase1-treated sections were used as positive control. (F) Quantification of experiment shown in E. Error bars, s.e.m. $^{**}P\leq0.01$ Student's *t*-test; n.s., not significantly different. (G) GFP expression in uninjured *runx2:GFP* transgenic fish is largely confined to the distalmost tips of the growing fin rays. prox., proximal. (H) Whole-mount *in situ* hybridization against *gfp* in *runx2:GFP* transgenic fish fin rays at 0 hpi and 1 dpi reveals induction of transgene expression at the fracture site (arrow). (I) Endogenous *runx2b* levels determined by qRT-PCR on fractured rays plus adjacent segments and normalized to the level at 0 hpi. Error bars, s.d. (J) Anti-Tenascin C and Zns5 antibody staining on cross-sections of three bony fin rays, the central ray of which had been fractured a day earlier. Tenascin C expression is present in osteoblasts and fibroblasts of the fractured fin ray (arrowhead) and extends into the fibroblast population of the interray (asterisks). (K) Magnified view of staining as in J. (L) Zns5+ osteoblasts in the proximity of the fracture incorporate BrdU (arrowheads). Longitudinal sections. (M) Quantification of experiment shown in L. BrdU+ Zns5+ cells were counted in bins of 175 µm. Gray dashed lines, segment boundaries. Error bars, s.e.m. $^{*}P\leq0.05$. $^{**}P\leq0.01$. $^{***}P\leq0.001$, Student's *t*-test. (N) Osteoblasts change their ultrastructure upon injury, determined by TEM. ECM, extracellular matrix; Nuc, nucleus/nuclei. *, artefact from staining procedure. Scale bars: 200 µm in A,G; 20 µm in D; 50 µm in E,H; 100 µm in J; 10 µm in K,L; 1 µm in N.

regulatory regions of the *entpd5* gene, an osteoblast-specific factor required for skeletal mineralization (Huitema et al., 2012). In adult caudal fins, *entpd5*:Kaede was expressed in osteoblasts in the center of each fin ray segment (Fig. 3A). We have previously shown that osteoblasts located at the segment centers are *osteocalcin*+ (Knopf et al., 2011), suggesting that *entpd5* expression in the adult fin is specific to mature osteoblasts. We first tested whether this line can be used to confirm osteoblast migration in response to fin amputation. Indeed, when we photoconverted osteoblasts from green to red in a single fin ray segment and amputated the fin in the adjacent segment, converted cells moved toward and beyond the amputation plane within 2 days (Fig. 3A; supplementary material Fig. S3, arrowhead).

We then photoconverted a population of osteoblasts in one fin ray segment, introduced a fracture in the same fin ray and followed osteoblast behavior by repeated imaging during the following days. When a fracture was introduced in the segment adjacent to the one with photoconverted cells (red line and right fin ray in Fig. 3B; supplementary material Fig. S3), these osteoblasts moved toward the fractured segment and crossed the segment boundary by 1 dpi (arrowheads in Fig. 3B; supplementary material Fig. S3). During the following day, photoconverted cells were present closer to the fracture site, and some reached the injured site at 3 dpi (right fin ray in Fig. 3B; supplementary material Fig. S3). By contrast, photoconverted osteoblasts one segment further away from the fracture did not change their position (blue line and blue asterisk in Fig. 3B; supplementary material Fig. S3). These results indicate that dedifferentiating osteoblasts in a distance of roughly one segment (about 350 µm) from the fracture start to move toward the injury within 24 h of the damage, which is similar to what we have observed during bone regeneration after amputation (Knopf et al., 2011).

Movement of osteoblasts toward the fracture could be due to active migration or passive displacement caused by cell proliferation. To distinguish between these possibilities, we performed live time-lapse confocal microscopy of photoconverted osteoblasts in *entpd5*:Kaede fish. We found that osteoblasts displayed dynamic cell morphology and that individual osteoblasts changed their position relative to other cells (Fig. 3C; supplementary material Movies 1 and 2). By contrast, osteoblasts showed no signs of motility in uninjured fin rays (supplementary material Movie 3). This strongly suggests that osteoblasts actively migrate toward a fracture.

To further confirm that osteoblasts move toward the fracture, we lineage traced *osterix*+ (*sp7* – ZFIN) osteoblasts. We used *osterix*:CreERT2-p2a-mCherry×*hsp70l*:*loxP* DsRed2 *loxP* nlsEGFP (in short *hs*:R to nG) double transgenic fish, in which 4-hydroxytamoxifen (4-HT)-induced Cre activity excises a *loxP*-flanked DsRed Stop cassette and thus allows for GFP expression in recombined cells and their progeny in response to heat shock (Halloran et al., 2000; Hans et al., 2009; Knopf et al., 2011). 4-HT treatment of adult fish before fracture resulted in stochastic labeling of osteoblasts with GFP after heat shock (Fig. 3D). Genetically labeled green cells accumulated in the area of the fracture callus within 2 dpi (Fig. 3D), indicating that *osterix*+ cells or their progeny move toward the injury site after fin ray fracture.

Redifferentiation of osteoblasts after fracture

We next characterized the temporal and spatial profiles of osteoblast redifferentiation during fracture healing and compared it to those observed in regenerating fins. Onset of osteogenesis as indicated by elevated GFP fluorescence in *runx2:GFP* transgenic fish occurred at the fracture site at the same time as in fin regenerates, namely at 2 days post amputation (dpa) and post injury (dpi), respectively (Fig. 3E; supplementary material Fig. S4A). Likewise, onset of osteoblast commitment, as indicated by *osterix*:nGFP expression, occurred at 3 days post lesion in both amputated and fractured fins (Fig. 3E; supplementary material Fig. S4B). The timing of late osteogenesis as indicated by reduced *runx2b* and increased *osteocalcin* expression (Hartmann, 2009), however, appeared to differ between regeneration after amputation and fracture repair. Although GFP reporter activity in *osteocalcin*:GFP transgenic fish was robustly induced at 6 dpa in regenerating fins, expression was only detected in about half of fractured rays at this time (arrow in Fig. 3E showing lack of expression versus arrowhead in supplementary material Fig. S4C showing presence of expression) and robust expression was detected in fractures only by 10 dpi. Concomitantly, while regenerating fins down-regulated *runx2:GFP* expression by 6 dpa, expression was maintained until 10 dpi in fractures (arrowhead in Fig. 3E; supplementary material Fig. S4A). We conclude that osteogenesis is initiated at the same speed in response to bone fractures and bone amputation, but that progression to mature osteoblasts is slower in fractures.

Osteoblast dedifferentiation occurs in injured skull bone

Having found that osteoblast dedifferentiation happens in response to fin ray fractures, we wondered whether it only occurs in lepidotrichia bones, which are specific to bony fishes and have no equivalent in mammals (Marí-Beffa et al., 2007). To test this, we assayed osteoblast behavior in response to injury of the dermal bone of the skull. We targeted the frontal and parietal bones of the zebrafish cranial vault, which are homologous to the corresponding

Development (2014) 141, 2225-2234 doi:10.1242/dev.105817

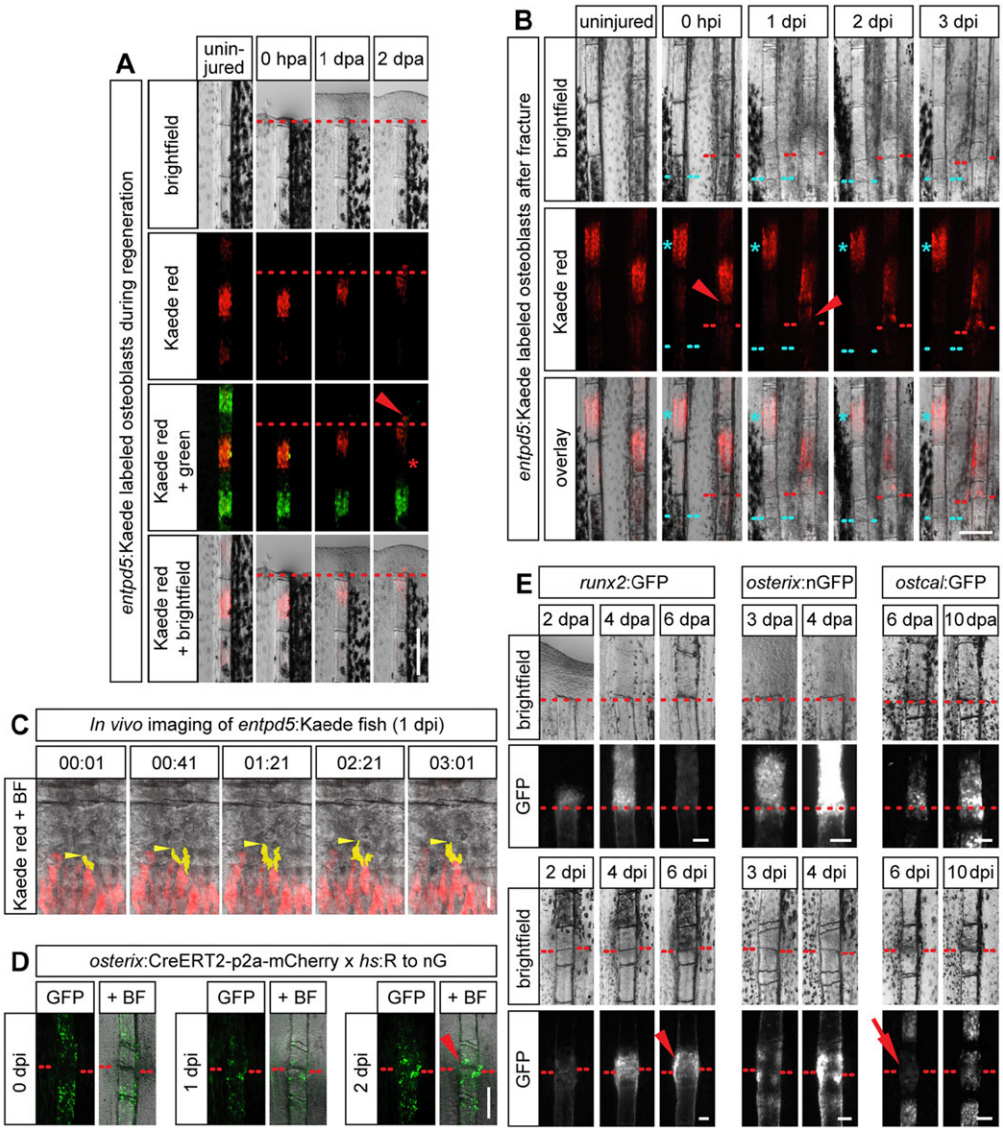

Fig. 3. Dedifferentiated osteoblasts migrate toward the injury site, where they redifferentiate. (A) *entpd5*:Kaede is expressed in mature osteoblasts in the center of the bony fin ray segments. In response to fin amputation, photoconverted osteoblasts (red) migrate to and beyond the amputation plane (arrowhead), as seen by repeated imaging of the same fish. At the same time the gap devoid of labeled osteoblasts at the segment boundary widens (asterisk). (B) Photoconverted osteoblasts in *entpd5*:Kaede transgenic fish in a segment adjacent to a fracture (right fin ray, arrowhead) or in the second segment from the fracture (left ray, asterisk). Osteoblasts migrate toward the fracture only from the segment adjacent to it. (C) Still images from a confocal time-lapse movie (supplementary material Movie 1) of migrating photoconverted Kaede+ osteoblasts in close proximity to the fracture. Protrusions of one cell are highlighted in yellow, its leading edge with an arrowhead. (D) *osterix*+ cells or their progeny accumulate at the fracture at 2 dpi (arrowhead), as revealed by stochastic Cre-mediated genetic labeling of osteoblasts in *osterix*:CreERT2-p2a-mCherry×*hs*:R to nG fish. (E) Comparison of transgene expression in *runx2:GFP*, *osterix*:nGFP and *osteocalcin*:GFP fins during regeneration after amputation (upper panels) versus repair after fracture (lower panels). *ostcal*, *osteocalcin*. Scale bars: 200 µm in A,B,D; 20 µm in C; 100 µm in E.

bones in the neurocranium of mammals. In analogy to established protocols for calvarial injuries in rodents (Spicer et al., 2012), we removed a circular piece of bone with a diameter of 0.5 mm by using a microdrill in the *os frontale* (Fig. 4A,B), although peripheral injury of the *os parietale* could sometimes not be avoided (Fig. 4A). These drill injuries healed quickly. By 3 dpi, small regions staining positive for both Alizarin Red and Calcein were detected in the injured area, suggesting new bone formation (Fig. 4B,C). By 7 dpi the lesions were almost completely filled with matrix, and by 14 dpi matrix formation as indicated by Calcein incorporation had largely returned to baseline levels (Fig. 4B,C).

We next injured the *os frontale* of *osteocalcin*:GFP transgenic fish to test whether mature osteoblasts downregulate *osteocalcin* expression. To reduce pigment obscuring the GFP signal, we introduced the *osteocalcin*:GFP line into the *casper* double mutant fish, which lack melanophores and iridophores (White et al., 2008). The GFP signal intensity in bone tissue close to the injured region was reduced at 3 dpi and more so at 7 dpi, as seen in whole-mount heads of live fish that were imaged repeatedly (Fig. 4D). GFP pixel intensity plots revealed that GFP intensity was significantly reduced up to a distance of at least 300 µm from the edge of the drill injury (Fig. 4E). Transverse cryosections immunostained with anti-Zns5 and anti-GFP antibodies revealed that uninjured skull bones were lined by a single layer of osteoblasts on both the external and internal surface of the bone (Fig. 4F). All osteoblasts staining positive for the pan-osteoblast marker Zns5 also appeared to be positive for *osteocalcin*:GFP, indicating that the vast majority of osteoblasts lining the adult skull bones are fully differentiated and that no or very few undifferentiated progenitors exist in these osteoblast layers (Fig. 4F). Sections spanning the border zone between noninjured bone and the drill hole (bracket in Fig. 4F,G) at 7 dpi revealed a thin layer of bone matrix in the injury area that was lined by a single layer of Zns5+ osteoblasts on both the external and internal surface (arrow in Fig. 4F) as well as Zns5+ osteoblasts lining the bone adjacent to the injury (arrowhead in Fig. 4F). Osteoblasts covering the newly formed bone in the injury were largely devoid of *osteocalcin*:GFP expression, indicating that these had not yet differentiated by 7 dpi (Fig. 4F). Intriguingly, *osteocalcin*:GFP expression was also weak in the osteoblasts lining the bone adjacent to the injury, being reduced to about 50% of the level detected in noninjured skull bones, confirming osteoblast dedifferentiation observed in live fish (Fig. 4F; supplementary material Fig. S5). At 7 dpi, osteoblasts in the injury area strongly expressed *runx2*:GFP (Fig. 4G), and *osterix*:nGFP at the periphery

Development (2014) 141, 2225-2234 doi:10.1242/dev.105817

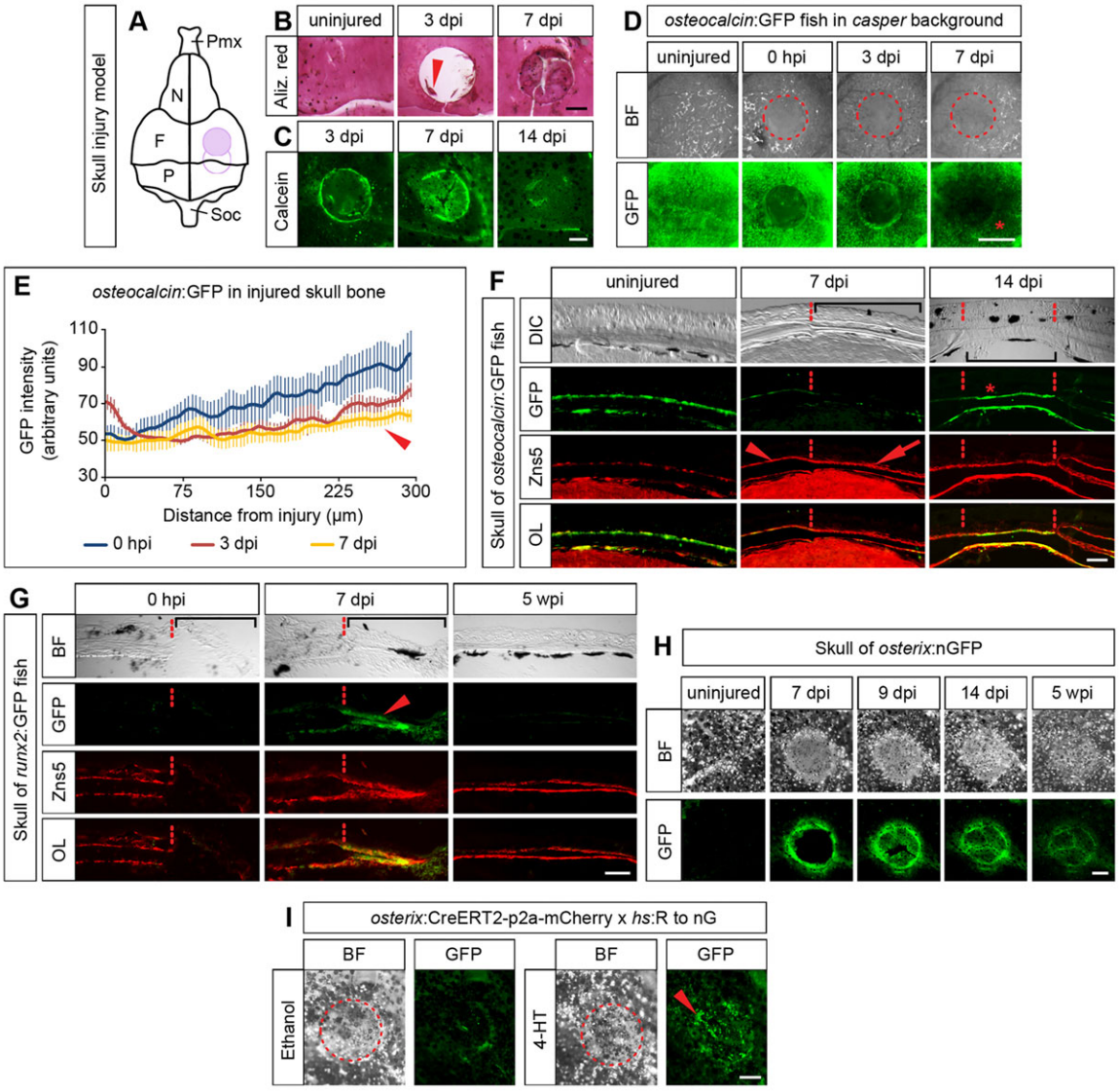

Fig. 4. Osteoblasts in dermal bone of the skull dedifferentiate following injury. (A) Scheme illustrating the bone injury (500 µm hole) in the *os frontale* (purple filled circle) or at the boundary between the *os frontale* and *os parietale* (empty circle) of the dorsal skull. F, *os frontale*; N, *os nasale*; P, *os parietale*; Pmx, *os praemaxillare*; Soc, *os supraoccipitale*. (B) Whole-mount view of uninjured and injured skulls at different times post injury stained with Alizarin Red. Arrowhead, islands of bone matrix. (C) Calcein staining of whole-mount injured skulls at different times post injury. (D) Reduction of GFP signal intensity in *osteocalcin*:GFP transgenic fish in proximity to the drill injury (asterisk), revealed by repeated live imaging of the same fish. (E) Quantification of experiment shown in D. Error bars, s.e.m. (F,G) Immunofluorescence of transverse sections of the dorsal skull stained for GFP and Zns5. Bracket, injury site; dashed line, injury boundary; arrowhead, osteoblasts in uninjured area; arrow, osteoblasts lining newly formed matrix in injury area. (F) *osteocalcin*:GFP fish. (G) *runx2*:GFP fish. Arrowhead, GFP+ osteoblasts lining newly formed matrix in injury area. (H) Skull of an *osterix*:nGFP fish before and after injury. (I) *osterix*+ osteoblasts contribute to repair of skull bone after injury. In *osterix*:CreERT2-p2a-mCherry×*hs*:R to nG double transgenic fish genetically labeled osteoblasts (bright nuclear signals) cover the injury site at 7 dpi (arrowhead). Only background fluorescence is detected in vehicle (ethanol)-treated fish. Scale bars: 200 µm in B,C,H,I; 500 µm in D; 50 µm in F,G.

of the injury (Fig. 4H). By 14 dpi, osteoblasts still expressed *osterix*:nGFP (Fig. 4H), but also had further matured as indicated by *osteocalcin*:GFP expression (Fig. 4F). Finally, by 5 weeks post injury, osteoblasts had ceased to express *runx2*:GFP (Fig. 4G) and displayed reduced *osterix*:nGFP expression (Fig. 4H).

We next tested whether surrounding *osterix*+ osteoblasts contribute to bone healing in the injured skull. After irreversible genetic labeling of adult osteoblasts in *osterix*:CreERT2-p2a-mCherry×*hs*:R to nG fish, we injured the zebrafish skull bone and checked for the presence of labeled osteoblasts in the injured area at 7 dpi. Whereas only background signal was observed in the vehicle-treated negative control, labeled osteoblasts characterized by nuclear GFP were found covering the injury in fish treated with 4-HT (Fig. 4I). This shows that *osterix*+ osteoblasts contribute to dermal bone repair in injured skull zebrafish skull bones.

Together, these data indicate that skull injuries heal via dedifferentiation of adjacently located mature osteoblasts, migration of dedifferentiated osteoblasts into the injury site and subsequent re-differentiation along the osteoblast lineage. Thus, osteoblast plasticity is not specific to lepidotrichia, but also occurs in dermal skull bone.

DISCUSSION

Our findings indicate that osteoblast dedifferentiation is neither restricted to the context of appendage regeneration nor to the special

Development (2014) 141, 2225-2234 doi:10.1242/dev.105817

bone type of lepidotrichia, but is likely to occur in response to internal injury of any dermal bone in zebrafish. Thus, mature fish osteoblasts display high plasticity and represent an important source of newly forming bone both after internal injury and appendage amputation. By contrast, differentiated osteoblasts in mammals are unlikely to be involved in bone repair. Although there is evidence for participation of postmitotic osteoblasts lining bone surfaces (bone lining cells) in mammalian bone formation after stimulation with either parathyroid hormone or FGF2 (Dobnig and Turner, 1995; Power et al., 2004; Kim et al., 2012), a recently developed microfracture model of the mouse calvaria and knee indicates that there is no or very low contribution of Osteocalcin+ cells to bone repair (Park et al., 2012). Rather, mesenchymal stem cells appear to be the precursors of newly forming osteoblasts during fracture repair in mammals (Park et al., 2012). Whether all osteoblasts in regenerating or healing fish bone are derived from mature cells via dedifferentiation remains to be shown; thus, a contribution of stem cells to fin regeneration or fracture repair cannot be ruled out. Of note, when osteoblasts are genetically depleted from zebrafish fins, bone can regenerate rather normally after amputation, implying that an alternative source of osteoblasts does exist; however, this has not been identified (Singh et al., 2012). Nevertheless, it is clear that in unperturbed conditions mature osteoblasts are an important source of healing bone in teleost fish, but not in mammals. It remains possible that in response to injury, mammalian mature osteoblasts do undergo dedifferentiation apparent by loss of *osteocalcin* and induction of *runx2* expression, yet they fail to migrate and do not contribute to injury repair. Adult mammalian skull-cap-derived osteoblasts reduce *osteocalcin* expression and re-enter the cell cycle when placed in culture (Lian and Stein, 1995), suggesting a dedifferentiation potential. Thus, it will be important to decipher the molecular mechanisms that allow for osteoblast dedifferentiation in zebrafish and to test whether the same mechanisms are able to induce osteoblast dedifferentiation in mammalian bone tissue, which could enhance bone healing. Considering both the speed of bone repair and the cost-efficiency of haltering zebrafish in the laboratory, we propose that skull injury models in zebrafish will, in addition to fin amputation and fracture, be very useful to investigate various aspects of vertebrate bone biology. Thus, the zebrafish injury models characterized here will aid in understanding the key mechanisms of bone repair and regeneration, one of which might be the plasticity of local differentiated bone cells.

MATERIALS AND METHODS

Fin amputations, fractures and skull injuries

Fin amputations were performed as previously described (Poss et al., 2000b) and fish were returned to 28.5°C water afterwards. To induce fin ray fractures, fish were anesthetized in 0.02% tricaine and placed laterally onto a 2% agarose-coated Petri dish. An injection needle (BD Becton Dickinson, 0.3×13 mm) was pushed onto the middle of a bony fin ray segment with slight pressure, until a transverse crack was introduced. A single fracture in the center of the fin ray segment was produced, which was usually limited to one of the two hemirays. Segments located three segments proximal to the bifurcation of the dorsal fin rays 3, 7 (sometimes 8, if fin ray 7 was heavily pigmented) and ventral fin ray 3 were chosen (usually three fractures per fish). Occasionally, we introduced a fourth and fifth fracture into the fins. For cryosections and qRT-PCR, up to eight (central) fin rays were fractured, whereas the outer ones were left untouched. Skull injuries were caused in anesthetized fish placed upright in a sponge using a microdrill (Fine Science Tools, 0.5 mm). All experiments with zebrafish were approved by the states of Saxony and Baden-Württemberg and performed in accordance to animal guidelines of TU Dresden and Ulm University.

Transgenic fish lines

The *osteocalcin*:GFP (*Ola.Osteocalcin.1*:EGFP^{hu4008}), *osterix*:nGFP (*Ola.Sp7*:nls-GFP^{zf132}), *runx2*:GFP (*Hsa.RUNX2-Mmu.Fos*:EGFP^{zf259}), *osterix*:CreERT2-p2a-mCherry (*Olsp7*:CreERT2-p2a-mCherry^{tud8}), *hs*:R to nG (*hsp70l*:*loxP* DsRed2 *loxP* nlsEGFP^{tud9}) and *keratin*:AmCyan [*keratin4*:irtTAM2(3F)-p2a-AmCyan^{ulm5}] fish lines have been described elsewhere (Knopf et al., 2011; Wehner et al., 2014). Creation of the *entpd5*:Kaede fish line was performed as described previously (Huitema et al., 2012; Bussmann and Schulte-Merker, 2011).

Quantification of GFP expression

Fin ray segments and skulls of live fish anesthetized with 0.02% tricaine were imaged repeatedly using identical settings. Pictures were acquired using a Leica MZ16 FA stereomicroscope equipped with a QIMAGING RETIGA-SRV camera. Intensity measurements along fin rays were made with the Plot profile tool in ImageJ Software version 1.45s along rectangular regions of interest whose width corresponded to that of individual fin rays. Intensity measurements with the Plot profile tool of injured heads in live fish were made along eight radial lines (anterior, anterior-left, left, posterior-left, posterior, posterior-right, right, anterior-right) starting from the edge of the injured bone. To quantify fluorescence on antibody-stained sections of injured skulls, intensity measurements were made along the stained tissue (curved lines, Plot profile tool). To normalize for differences in transgene expression levels between individual fish, all values were normalized against the average pixel intensity of uninjured sections.

Conversion of Kaede and *in vivo* imaging of *entpd5*:Kaede fish

To convert Kaede+ cells from green to red fluorescence, distinct fin ray segments of anesthetized *entpd5*:Kaede fish were illuminated with a UV laser (100% intensity, 400 Hz, frame averaging 14 times) connected to a Leica SP5 I confocal laser scanning microscope. After documentation of the converted cells with the stereomicroscope, fin ray fractures were introduced in adjacent segments or segments located two segments apart. Fin rays were imaged during the following days to reveal migration of converted cells. For *in vivo* imaging, fish were anesthetized and immobilized by covering the trunk and tail fin with 2% agarose. Fish were intubated with tubing (polyethylene tubing PE-160/10, OD=1.57 mm, ID=1.14 mm, Harvard Apparatus) which was connected to fresh fish system water and 0.02% tricaine, respectively. Depending on the intensity of gill movements fish were either supplied with pure system water or tricaine solution. Image aquisition was performed every 5 or 20 min, respectively, using a Leica SP5 confocal microscope equipped with a 20× dipping lens.

Osteoblast fate mapping

Olsp7:CreERT2-p2a-mCherry^{tud8}; *hsp70l*:*loxP* DsRed2 *loxP* nlsEGFP^{tud9} double transgenic fish were injected intraperitoneally either once (fin ray fractures) or repeatedly on three consecutive days (skull injuries) with 10 µl of 2.5 µM 4-hydroxytamoxifen (Sigma) or with the vehicle control ethanol. Seven days later fish were heat shocked at 37°C for 1 h and roughly 12 h later analyzed for recombination by the appearance of GFP+ cells. Fish were injured and photographed right after the insult (0 hpi) and at different time points post-injury. Fish were heat shocked roughly 12 h before each imaging to reveal GFP+ cells.

Proliferation studies with BrdU

Fish were incubated in 5 mM 5-bromo-2-deoxyuridine (Sigma) in fish system water for 8 h, after which the fins were fixed in 4% PFA.

Immunofluorescence

Fin and head cryosections were prepared as described (Knopf et al., 2011; Grandel et al., 2006). Immunofluorescence on fin cryosections was performed according to Knopf et al. (2011). A similar protocol was performed on skull cryosections (14 µm), except that the methanol treatment and blocking with calf plus horse serum were omitted. Antibodies used are listed by Knopf et al. (2011). In addition, rabbit anti-Osteocalcin (anti-ArBGP, gift of ML Cancela, Centre of Marine Sciences, Faro,

Development (2014) 141, 2225-2234 doi:10.1242/dev.105817

Portugal) was used at 1:250. Detection of BrdU was performed as described (Knopf et al., 2011).

In situ hybridizations

Chromogenic whole-mount *in situ* hybridization was performed according to Knopf et al. (2011). Fluorescent whole-mount *in situ* hybridization was performed with the TSA Plus kit (Perkin Elmer) according to the manufacturer's instructions.

In situ hybridization on cryosections was performed as follows: slides were dried for 1-3 h at room temperature (RT), treated with ice-cold MetOH for 15 min, rehydrated with TBST (15 mM NaCl, 5 mM Tris, 0.1% Tween 20, pH 7.5) twice for 10 min each, incubated with Proteinase K (5 µg/ml; Invitrogen) in TBST for 10 min, washed with TBST four times for 5 min each. Slides were then incubated with denatured probe (70°C for 10 min, then put on ice) against *amCyan* mRNA at 55°C o/n in a humidified chamber containing Solution A (150 mM NaCl, 15 mM natriumcitrate, pH 6, 50% deionized formamide, 0.1% Tween 20). Slides were washed with Solution A three times (1×15 min, 2×30 min) at 55°C, followed by two washes for 30 min each with TBST at RT. Sections were blocked in 10% NCS (newborn calf serum, Sigma Aldrich) in TBST for at least 1 h at RT, incubated with anti-Dig-AP coupled antibody (Roche) at 1:2000 in 10% FCS in TBST o/n at 4°C. Slides were then washed with TBST four times for 30 min each, equilibrated with freshly prepared NTMT (100 mM Tris HCl pH 9.5, 50 mM $MgCl_2$, 100 mM NaCl, 0.1% Tween 20) and incubated in the dark with staining solution [400 µl/slide containing 1.4 µl NBT and 2.7 µl BCIP (both Roche) in NTMT]. Staining was stopped with four washes of PBT (10 min each) and slides were postfixed with 4% PFA in PBS for 15 min at RT or at 4°C o/n. Slides were washed with PBS and mounted with 70% glycerol.

Staining with AFOG, Alizarin Red/Alcian Blue and Calcein, and TEM

To stain sections with AFOG, slides were dried at RT for 1-2 h, incubated in Bouin's solution first for 2 h in 60°C, then for an additional 60 min at RT. Slides were washed in running water for 30 min, rinsed in 1% phosphomolybdic acid for 5 min and washed in dH_2O for 4-5 min, after which they were placed in AFOG staining solution (1 g Analine Blue, 2 g Orange G, 3 g Acid Fuchsin in 200 ml dH_2O, pH 1.09) for 4-5 min. Slides were rinsed in dH_2O for 2 min, dehydrated in 2×5 min 95% and 100% ethanol each, placed in Xylen for 2×2 min and embedded with Cytoseal.

Combined Alizarin Red/Alcian Blue staining was performed on methanol-treated (series of 70, 50 and 30% in PBS) fins. After rehydration with PBS for 2×20 min and water for 5 min, fins were stained with Alcian Blue (Sigma Aldrich) staining solution (Part A: 0.02% Alcian Blue in 50 mM $MgCl_2$) for 2 h at RT. Fins were then treated with an ethanol series (90, 50 and 30% in 50 mM $MgCl_2$) and washed for 2 h in water. Alizarin Red (Sigma Aldrich) staining solution (Part B: 0.5% Alizarin Red in 10% glycerol) was added to the fins and incubated for 1 h. Fins were cleared with a decreasing potassium hydroxide:glycerol series (3:1 o/n, 1:1 o/n, 1:3 o/n) and mounted with 80% glycerol for imaging. Fins were then embedded for cryosectioning (see above).

To detect calcium deposition in fin fractures and skull injuries, live fish were incubated for 20 min in 100 ml of 0.2% Calcein (Sigma Aldrich) in dH_2O (pH 7.5), rinsed in water once and washed in water for additional 20 min.

Toluidine Blue staining and TEM were performed according to Knopf et al. (2011).

Quantitative PCR (qRT-PCR)

For qRT-PCR eight central bony fin rays were fractured approximately three segments proximal to the bifurcation point (12 fish per sample). The fractured plus the two adjacent segments were harvested using a scalpel. RNA isolation, cDNA transcription and determination of relative mRNA expression was performed as described previously (Knopf et al., 2011). For quantitative PCR of *runx2b* the following intron spanning primers were used: 171 bp; ACACCCAGACCCTCACTCAG; GACAGCGGAGTGGTGGAG.

TUNEL assay

TUNEL staining on cryosections was performed with the ApopTag Red *In Situ* Apoptosis Detection Kit (Millipore) according to the manufacturer's instructions. *osterix*:nGFP (*OlSp7*:nlsGFP^{zf132}) fish were used, in which osteoblasts are labeled by nuclear GFP. GFP was visualized by immunofluorescent anti-GFP staining (see above) preceding the TUNEL assay.

Necrosis staining

Necrotic cells were detected as described with modifications (Roger et al., 1996). In brief, live fish with fractured fin rays were incubated for 20 min in 100 µg/ml Acridine Orange stock solution (Sigma Aldrich) and 2 µg/ml ethidium bromide (Roth). Fish were washed twice for 20 min in PBS, after which they were transferred to fishwater for another 20 min. Fins were fixed in 4% PFA for several hours at RT, washed several times with PBS and imaged with a Leica SP5 confocal microscope. Necrotic cells incorporate both Acridine Orange and ethidium bromide, and fluoresce brightly orange (Roger et al., 1996; Renvoize et al., 1998; Watanabe et al., 2007).

Statistics and experimental numbers

Information on sample sizes and further statistical information can be found for all experiments in supplementary material Tables S1 and S2.

Acknowledgements

We thank A. Chekuru and J. Kaslin for their help in establishing the fracture and drill injury methods, M. Fischer, K. Sippel, J. Michel for excellent fish care, and T. Kurth for technical support. We are grateful to L. Cancela (Faro, Portugal) for sharing the anti-ArBGP (Ocn) antiserum, and to F. Argenton (Padova, Italy) and M. Brand (Dresden, Germany) for sharing transgenic fish.

Competing interests

The authors declare no competing financial interests.

Author contributions

K.G., F.K. and D.W. performed experiments and analyzed data. F.K. and G.W. designed experiments and wrote the paper. L.F.A.H. and S.S.-M. supplied unpublished fish lines.

Funding

This work was supported by a grant of the Deutsche Forschungsgemeinschaft [DFG WE 4223/3-1 to G.W.]. S.S.-M. is supported by the Royal Netherlands Academy of Arts and Sciences (KNAW).

Supplementary material

Supplementary material available online at
http://dev.biologists.org/lookup/suppl/doi:10.1242/dev.105817/-/DC1

References

Barnes, G. L., Kostenuik, P. J., Gerstenfeld, L. C. and Einhorn, T. A. (1999). Growth factor regulation of fracture repair. *J. Bone Miner. Res.* **14**, 1805-1815.

Bussmann, J. and Schulte-Merker, S. (2011). Rapid BAC selection for tol2-mediated transgenesis in zebrafish. *Development* **138**, 4327-4332.

Cameron, J. A., Milner, D. J., Lee, J. S., Cheng, J., Fang, N. X. and Jasiuk, I. M. (2013). Employing the biology of successful fracture repair to heal critical size bone defects. *Curr. Top. Microbiol. Immunol.* **367**, 113-132.

Chiquet-Ehrismann, R. and Tucker, R. P. (2004). Connective tissues: signalling by tenascins. *Int. J. Biochem. Cell Biol.* **36**, 1085-1089.

Conaway, H. H., Henning, P. and Lerner, U. H. (2013). Vitamin A metabolism, action, and role in skeletal homeostasis. *Endocr. Rev.* **34**, 766-797.

Constantine, V. S. and Mowry, R. W. (1968). Selective staining of human dermal collagen. I. An analysis of standard methods. *J. Invest. Dermatol.* **50**, 414-418.

Dobnig, H. and Turner, R. T. (1995). Evidence that intermittent treatment with parathyroid hormone increases bone formation in adult rats by activation of bone lining cells. *Endocrinology* **136**, 3632-3638.

Gavaia, P. J., Simes, D. C., Ortiz-Delgado, J. B., Viegas, C. S. B., Pinto, J. P., Kelsh, R. N., Sarasquete, M. C. and Cancela, M. L. (2006). Osteocalcin and matrix Gla protein in zebrafish (Danio rerio) and Senegal sole (Solea senegalensis): comparative gene and protein expression during larval development through adulthood. *Gene Expr. Patterns* **6**, 637-652.

Grandel, H., Kaslin, J., Ganz, J., Wenzel, I. and Brand, M. (2006). Neural stem cells and neurogenesis in the adult zebrafish brain: origin, proliferation dynamics, migration and cell fate. *Dev. Biol.* **295**, 263-277.

Hall, B. K. (2005). *Bones and Cartilage: Developmental and Evolutionary Skeletal Biology*. San Diego: Elsevier Academic Press.
Halloran, M. C., Sato-Maeda, M., Warren, J. T., Su, F., Lele, Z., Krone, P. H., Kuwada, J. Y. and Shoji, W. (2000). Laser-induced gene expression in specific cells of transgenic zebrafish. *Development* **127**, 1953-1960.
Han, M., Yang, X., Taylor, G., Burdsal, C. A., Anderson, R. A. and Muneoka, K. (2005). Limb regeneration in higher vertebrates: developing a roadmap. *Anat. Rec. B New Anat.* **287B**, 14-24.
Hans, S., Kaslin, J., Freudenreich, D. and Brand, M. (2009). Temporally-controlled site-specific recombination in zebrafish. *PLoS ONE* **4**, e4640.
Hartmann, C. (2009). Transcriptional networks controlling skeletal development. *Curr. Opin. Genet. Dev.* **19**, 437-443.
Huitema, L. F. A., Apschner, A., Logister, I., Spoorendonk, K. M., Bussmann, J., Hammond, C. L. and Schulte-Merker, S. (2012). Entpd5 is essential for skeletal mineralization and regulates phosphate homeostasis in zebrafish. *Proc. Natl. Acad. Sci. U.S.A.* **109**, 21372-21377.
Johnson, S. L. and Weston, J. A. (1995). Temperature-sensitive mutations that cause stage-specific defects in Zebrafish fin regeneration. *Genetics* **141**, 1583-1595.
Kim, S. W., Pajevic, P. D., Selig, M., Barry, K. J., Yang, J.-Y., Shin, C. S., Baek, W.-Y., Kim, J.-E. and Kronenberg, H. M. (2012). Intermittent parathyroid hormone administration converts quiescent lining cells to active osteoblasts. *J. Bone Miner. Res.* **27**, 2075-2084.
Knopf, F., Hammond, C., Chekuru, A., Kurth, T., Hans, S., Weber, C. W., Mahatma, G., Fisher, S., Brand, M., Schulte-Merker, S. et al. (2011). Bone regenerates via dedifferentiation of osteoblasts in the zebrafish fin. *Dev. Cell* **20**, 713-724.
Komatsu, D. E., Mary, M. N., Schroeder, R. J., Robling, A. G., Turner, C. H. and Warden, S. J. (2010). Modulation of Wnt signaling influences fracture repair. *J. Orthop. Res.* **28**, 928-936.
Lee, Y., Hami, D., De Val, S., Kagermeier-Schenk, B., Wills, A. A., Black, B. L., Weidinger, G. and Poss, K. D. (2009). Maintenance of blastemal proliferation by functionally diverse epidermis in regenerating zebrafish fins. *Dev. Biol.* **331**, 270-280.
Lian, J. B. and Stein, G. S. (1995). Development of the osteoblast phenotype: molecular mechanisms mediating osteoblast growth and differentiation. *Iowa Orthop. J.* **15**, 118-140.
Marí-Beffa, M., Santamaría, J. A., Murciano, C., Santos-Ruiz, L., Andrades, J. A., Guerado, E. and Becerra, J. (2007). Zebrafish fins as a model system for skeletal human studies. *ScientificWorldJournal* **7**, 1114-1127.
Monaghan, J. R. and Maden, M. (2013). Cellular plasticity during vertebrate appendage regeneration. *Curr. Top. Microbiol. Immunol.* **367**, 53-74.
Moro, E., Ozhan-Kizil, G., Mongera, A., Beis, D., Wierzbicki, C., Young, R. M., Bournele, D., Domenichini, A., Valdivia, L. E., Lum, L. et al. (2012). In vivo Wnt signaling tracing through a transgenic biosensor fish reveals novel activity domains. *Dev. Biol.* **366**, 327-340.
Nagamine, T., Imamura, T., Ishidou, Y., Kato, M., Murata, F., ten Dijke, P. and Sakou, T. (1998). Immunohistochemical detection of activin A, follistatin, and activin receptors during fracture healing in the rat. *J. Orthop. Res.* **16**, 314-321.
Park, D., Spencer, J. A., Koh, B. I., Kobayashi, T., Fujisaki, J., Clemens, T. L., Lin, C. P., Kronenberg, H. M. and Scadden, D. T. (2012). Endogenous bone marrow MSCs are dynamic, fate-restricted participants in bone maintenance and regeneration. *Cell Stem Cell* **10**, 259-272.
Pereira, B. P., Zhou, Y., Gupta, A., Leong, D. T., Aung, K. Z., Ling, L., Pho, R. W. H., Galindo, M., Salto-Tellez, M., Stein, G. S. et al. (2009). Runx2, p53, and pRB status as diagnostic parameters for deregulation of osteoblast growth and differentiation in a new pre-chemotherapeutic osteosarcoma cell line (OS1). *J. Cell Physiol.* **221**, 778-788.
Poss, K. D., Shen, J. and Keating, M. T. (2000a). Induction of *lef1* during zebrafish fin regeneration. *Dev. Dyn.* **219**, 282-286.
Poss, K. D., Shen, J., Nechiporuk, A., McMahon, G., Thisse, B., Thisse, C. and Keating, M. T. (2000b). Roles for Fgf signaling during zebrafish fin regeneration. *Dev. Biol.* **222**, 347-358.
Power, R. A., Iwaniec, U. T., Magee, K. A., Mitova-Caneva, N. G. and Wronski, T. J. (2004). Basic fibroblast growth factor has rapid bone anabolic effects in ovariectomized rats. *Osteoporos. Int.* **15**, 716-723.
Renvoizé, C., Biola, A., Pallardy, M. and Breard, J. (1998). Apoptosis: identification of dying cells. *Cell Biol. Toxicol.* **14**, 111-120.
Roger, R., Issaad, C., Pallardy, M., Leglise, M. C., Turhan, A. G., Bertoglio, J. and Breard, J. (1996). BCR-ABL does not prevent apoptotic death induced by human natural killer or lymphokine-activated killer cells. *Blood* **87**, 1113-1122.
Sandoval-Guzmán, T., Wang, H., Khattak, S., Schuez, M., Roensch, K., Nacu, E., Tazaki, A., Joven, A., Tanaka, E. M. and Simon, A. (2014). Fundamental differences in dedifferentiation and stem cell recruitment during skeletal muscle regeneration in two salamander species. *Cell Stem Cell* **14**, 174-187.
Satoh, A., Cummings, G. M. C., Bryant, S. V. and Gardiner, D. M. (2010). Neurotrophic regulation of fibroblast dedifferentiation during limb skeletal regeneration in the axolotl (Ambystoma mexicanum). *Dev. Biol.* **337**, 444-457.
Schmid, G. J., Kobayashi, C., Sandell, L. J. and Ornitz, D. M. (2009). Fibroblast growth factor expression during skeletal fracture healing in mice. *Dev. Dyn.* **238**, 766-774.
Singh, S. P., Holdway, J. E. and Poss, K. D. (2012). Regeneration of amputated zebrafish fin rays from de novo osteoblasts. *Dev. Cell* **22**, 879-886.
Sousa, S., Afonso, N., Bensimon-Brito, A., Fonseca, M., Simoes, M., Leon, J., Roehl, H., Cancela, M. L. and Jacinto, A. (2011). Differentiated skeletal cells contribute to blastema formation during zebrafish fin regeneration. *Development* **138**, 3897-3905.
Sousa, S., Valerio, F. and Jacinto, A. (2012). A new zebrafish bone crush injury model. *Biol. Open* **1**, 915-921.
Spicer, P. P., Kretlow, J. D., Young, S., Jansen, J. A., Kasper, F. K. and Mikos, A. G. (2012). Evaluation of bone regeneration using the rat critical size calvarial defect. *Nat. Protoc.* **7**, 1918-1929.
Tanaka, E. M. and Reddien, P. W. (2011). The cellular basis for animal regeneration. *Dev. Cell* **21**, 172-185.
Watanabe, N., Hirayama, R. and Kubota, N. (2007). The chemopreventive flavonoid apigenin confers radiosensitizing effect in human tumor cells grown as monolayers and spheroids. *J. Radiat. Res.* **48**, 45-50.
Wehner, D., Cizelsky, W., Vasudevaro, M. D., Ozhan, G., Haase, C., Kagermeier-Schenk, B., Röder, A., Dorsky, R. I., Moro, E., Argenton, F. et al. (2014). Wnt/beta-catenin signaling defines organizing centers that orchestrate growth and differentiation of the regenerating zebrafish caudal fin. *Cell Rep.* **6**, 467-481.
White, R. M., Sessa, A., Burke, C., Bowman, T., LeBlanc, J., Ceol, C., Bourque, C., Dovey, M., Goessling, W., Burns, C. E. et al. (2008). Transparent adult zebrafish as a tool for in vivo transplantation analysis. *Cell Stem Cell* **2**, 183-189.

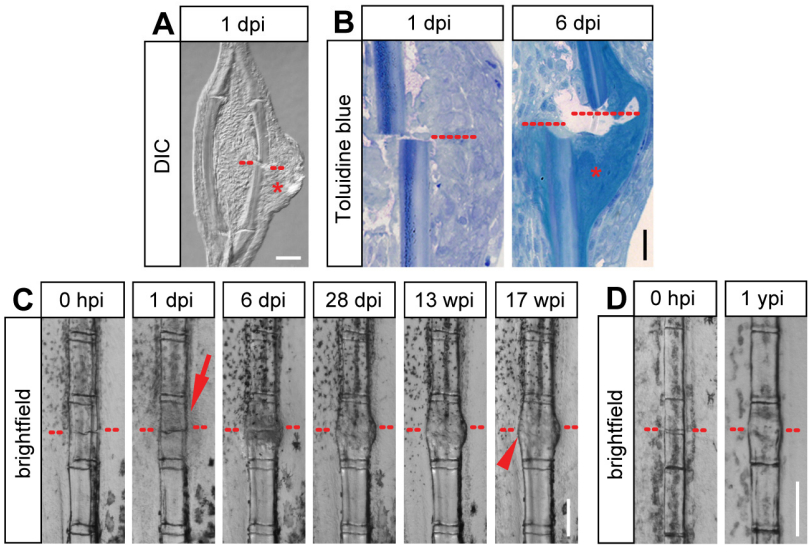

Fig. S1. Soft and hard callus formation in fractured fin rays.

(**A**) Longitudinal section view of a fractured fin ray at 1 dpi. The fracture site is indicated by the red dashed line. A swelling covering the fractured hemiray is visible (asterisk). Scale bar, 50 µm. DIC, differential interference contrast. dpi, day post injury.

(**B**) Toluidine blue stained sections of fractured fin hemirays at 1 dpi and 6 dpi. At 6 dpi, collagenous tissue has accumulated at the fracture site (asterisk). Scale bar, 30 µm.

(**C**) Bone fractures in the fin ray heal, however the bone keeps a thickened appearance up to at least 4 months post injury. Live whole mount view of the same fin ray at different time points post fracture. The epidermal thickening forming at 1 dpi is indicated by the arrow. The thickened appearance of the fractured segment is indicated by the arrowhead. Scale bar, 200 µm. hpi, hours post injury. wpi, weeks post injury.

(**D**) The fractured fin ray segment is distinguishable from neighboring unfractured segments at 1 year post injury (ypi). Live whole mount view of the same fin ray at 0 hpi and 1 year later. The thickened bone is indicated by the arrowhead. Scale bar, 200 µm.

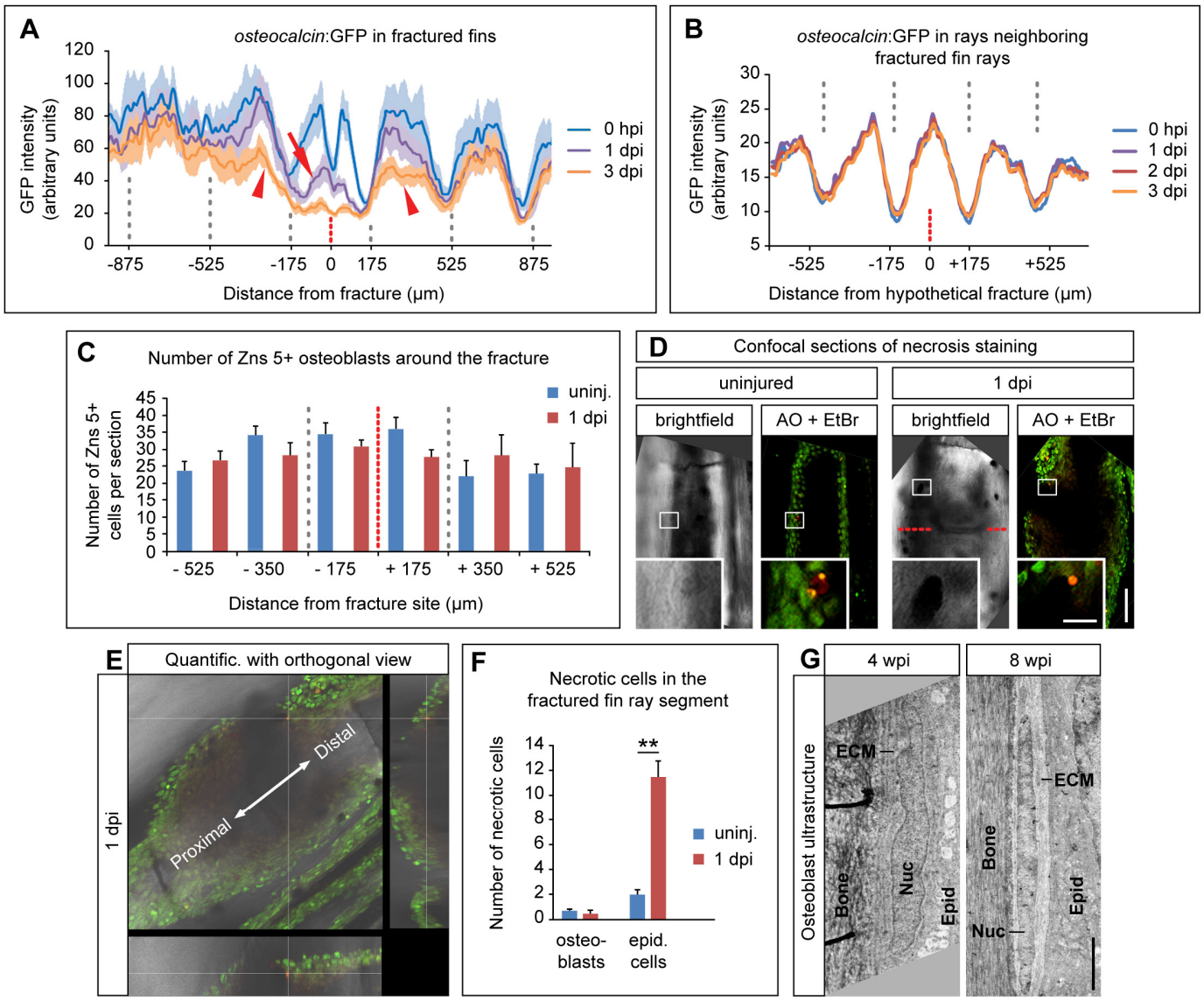

Fig. S2. Osteoblasts do not die after fracture and *osteocalcin* downregulation is not a systemic effect.

(**A**) GFP intensity plot illustrating reduced levels of GFP in the fractured (arrow) and adjacent (arrowheads) segments after injury at 1 and 3 dpi. The grey dashed lines indicate segment boundaries, while the red dashed line indicates the fracture site. Average GFP intensity ± s.e.m. is shown. dpi, day(s) post injury. hpi, hours post injury.

(**B**) *osteocalcin*:GFP downregulation is not a systemic response. GFP intensity measurements in uninjured fin rays neighboring fractured fin rays reveal that there is no reduction of GFP signal after injury.

(**C**) The number of Zns5+ osteoblasts is not significantly altered at 1 dpi when compared to uninjured fins. Absolute numbers of osteoblasts per longitudinal section in bins of 175 µm along the fractured fin ray are shown. There are no significant differences (Student's t-test) in the respective uninjured versus 1 dpi groups. Note that 1 fin ray segment is approximately 350 µm long. Error bars, s.e.m. uninj. = uninjured.

(**D**) Confocal (optical section) view of an uninjured versus 1 dpi whole mount fin ray stained for necrotic cells using acridine orange and ethidium bromide Necrotic cells are labeled in both green (acridine orange) and red (ethidium bromide) at the same time. Necrosis of osteoblasts is a rare event both in uninjured and injured fin rays. One necrotic osteoblast in each example is shown in the magnified view. Osteoblasts were identified by their position in the cell layer directly abutting the bone matrix. Scale bar (overview), 50 µm. Scale bar (magnified view), 10 µm. AO = acridine orange. EtBr = Ethidium bromide.

(**E**) Orthogonal view method used for quantification of necrotic cells on confocal (optical) sections. Depending on the location of the necrotic cell either close to the surface (epidermal cell layers) or the deeper bone matrix (osteoblast cell layers) necrotic cells were counted as either epidermal cells or osteoblasts. The example shown here represents a necrotic osteoblast. Quantific. = quantification.

(**F**) Quantification of the experiments depicted in (D) and (E). While osteoblast necrosis is unchanged after fin ray fracture, epidermal cells undergo significantly enhanced necrosis after injury. Error bars, s.e.m. **, $p \leq 0.01$, Student's t-test. (**G**) Osteoblasts keep a rounded morphology and ultrastructure indicative of bone matrix production for at least 4 weeks post injury, and adopt their original elongated appearance only some weeks later. Electron micrographs of osteoblasts at 4 and 8 wpi. Scale bar, 2 µm. ECM = extracellular matrix, Epid = epidermis, Nuc = nucleus.

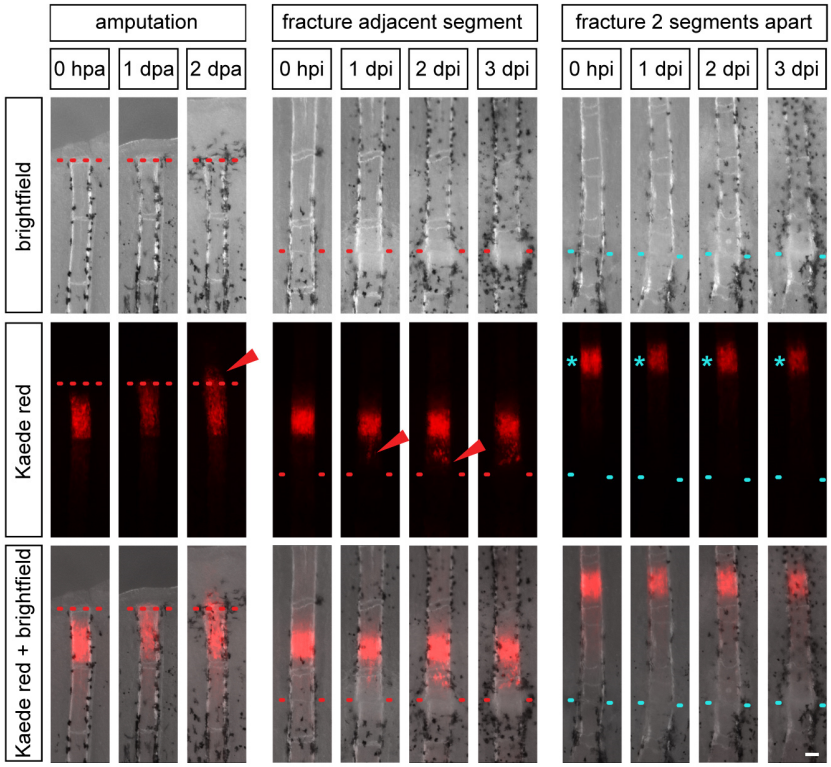

Fig. S3. Dedifferentiated osteoblasts migrate to the site of injury.

Individual *entpd*5:Kaede fish were repeatedly imaged at the indicated time points. Left: In response to fin amputation, photoconverted osteoblasts of *entpd5*:Kaede transgenic fish (red) migrate to and beyond the amputation plane (arrowhead) as seen by repeated imaging of the same fish. Middle: Photoconverted osteoblasts in a segment adjacent to a fracture migrate towards the fracture (arrowhead). Right: Photoconverted osteoblasts in the second segment from the fracture do not change position. Red and blue dotted lines, fracture. Scale bar, 100 µm.

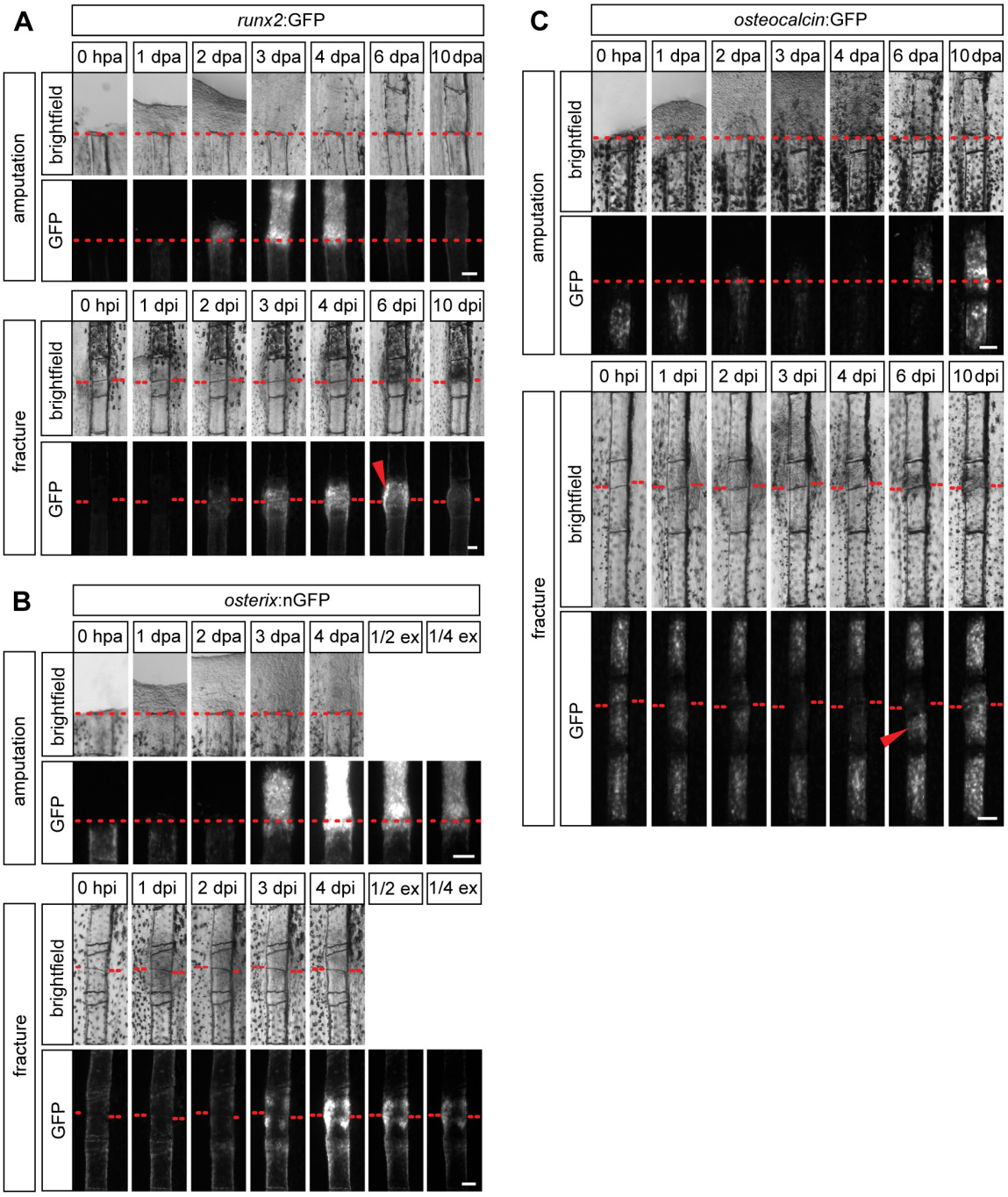

Fig. S4. Timing of osteogenesis is similar in fractured versus amputated fin rays, but progression to late osteoblasts is delayed in fractures.

(**A**) Time course of transgene expression in *runx2*:GFP fins during regeneration after amputation versus repair after fracture. GFP fluorescence is visible from 2 dpa/i in both injury models. *runx2*:GFP expression is reduced again to levels of uninjured fins at 6 dpa, while it is still high at this time point in fractured fin rays (arrowhead).

(**B**) Time course of transgene expression in *osterix*:nGFP fins. GFP fluorescence is visible at 3 dpa/i in a similar intensity and is increased at 4 dpa/i in both injury models. ex, exposure.

(**C**) Time course of transgene expression in *osteocalcin*:GFP fins. GFP fluorescence drops after injury up to 4 dpa/i in both injury models and recurs at 6 dpa in regenerating fins. In fractured fin rays expression levels are equally re-induced at 6 dpi in half of the cases looked at (arrowhead). GFP fluorescence throughout the fractured segment is completely re-established at 10 dpi. dpa, day(s) post amputation. dpi, day(s) post injury.

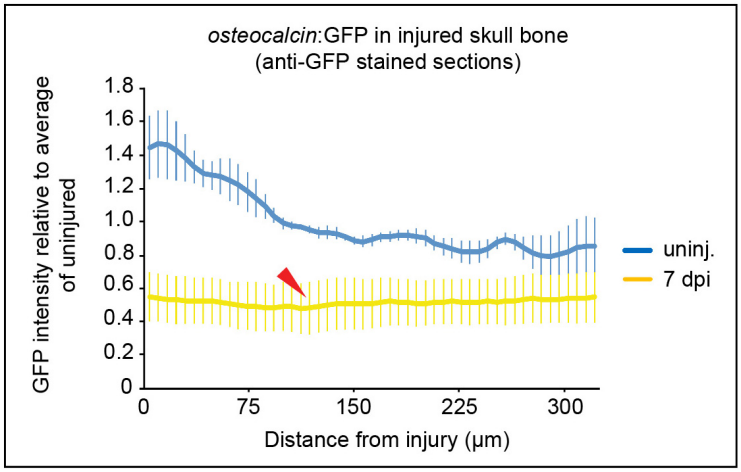

Fig. S5. Osteoblasts reduce *osteocalcin* promoter activity after skull bone injury.

Osteoblasts in the proximity to the skull injury site reduce *osteocalcin* promoter activity as indicated by reduction of GFP signal intensity in *osteocalcin*:GFP transgenic fish. Quantification of GFP signal intensity on anti-GFP antibody stained cryosections of uninjured versus 7 dpi skulls. GFP signal intensity around the injury site is reduced at 7 dpi (arrowhead). Average intensity of plots along the bone surface (normalized to the average intensity of uninjured) ± s.e.m. is shown.

Movie 1. Osteoblasts migrate to the fracture site.

In vivo confocal time lapse movie (image acquisition every 20 min for roughly 3 hours in a single z-plane) showing osteoblasts close to a fin fracture. Osteoblasts are labeled by Kaede which was light-converted from green to red fluorescence before fracture. The cell protrusions of a single osteoblast are false-coloured in translucent purple to illustrate their dynamic motion in direction of the fracture.

Movie 2. Osteoblasts migrate to the fracture site.

Second example of an in vivo confocal time lapse movie (image acquisition every 5 min for 4 hours in a single z-plane) showing Kaede (red)+ osteoblasts close to a fin fracture. Movement of one osteoblast traversing the joint between unfractured and fractured segment is highlighted by the arrowhead.

Movie 3. Osteoblasts are not motile in uninjured fin rays.

In vivo confocal time lapse movie (image acquisition every 20 min for nearly 4 hours in a single z-plane) showing osteoblasts in an uninjured fin ray. Kaede (red)+ osteoblasts are devoid of motile cell protrusions and appear round rather than elongated. Movement of the fish resulted in occasional shifts of the z-plane, however, osteoblasts appear not to change their position relative to each other or the underlying bone matrix and segment joints.

Movie 1.

Movie 2.

Movie 3.

Table S1. Experimental numbers for main figures

Figure	Experimental Numbers
1A	n = 5 fish, 14/15 rays with epidermal callus; 14/15 rays with 'hard callus' at 6 dpi; 13/15 rays thickened appearance wo. visible crack
1B	n = 5 fish, 22 rays (uninjured) & 23 rays (1 dpi), 22/22 sections (uninjured) epidermis stained, 12/23 sections (1 dpi) whole thickening positive for amcyan, 11/23 sections (1 dpi) part of thickening overlying fracture positive for amCyan
1C	n = 3 fish, 3 rays, 7/7 sections with blue (collagen+) hard callus at fracture
1D	n = 2 fish, 8/8 rays with Aliz.red+ callus but no alcian blue
1E	n = 2 fish, 11/11 rays with Calcein+ callus
1F	n = 3 fish, 5 rays (uninjured) & 5 rays (6 dpi) analyzed, 18/18 sections (uninjured) with Osteocalcin protein in bone matrix; 13/13 sections (6 dpi) with callus devoid of Osteocalcin protein
1G	n = 3 fish, 5 rays, 13/14 sections with Osteocalcin protein in callus
1H	n = 3 fish with 5 rays (uninjured) / 3 fish with 5 rays (6 dpi) / 4 fish with 6 rays (28 dpi), 16/16 sections without fracture (uninjured); 10/10 sections fracture ends not rejoined and callus bridging (6dpi); 15/16 sections fracture ends not rejoined (28 dpi)
1I	n = 4 fish with 10/10 rays without signal (0 hpi) / 5 fish with 8/10 rays with signal (3 dpi)
1J	n = 6 fish with 10 or more rays (3 dpa) / 3 fish with 9 rays (3 dpi), 6/6 fish with signal (3 dpa), 9/9 rays without signal (3 dpi)
1K	n = 5 fish each, 8/8 rays (0hpi) without signal; 7/9 rays (3 dpi) with signal
1L	n = 4 fish with 9/9 rays without signal (0 hpi) / 5 fish with 10/10 rays with signal (1 dpi)
1M	n = 5 fish each with 15/15 rays without signal (0 hpi) / 15/15 rays with signal (2 dpi)
1N	n = 4 fish, 8/8 rays without signal (0 hpi); 8/8 rays with signal (3 dpi)

2A-B	n = 5 fish with 15 rays (Plot profile tool ImageJ)
2D	n = 3 fish with 3 rays (uninjured & 3 dpi each), 9/9 sections with GFP in osteoblasts (uninjured), 11/13 sections without GFP signal close to fracture (3 dpi)
2E-F	n = 2 fish with 2 rays with 45 sections (uninjured) / 3 fish with 4 rays with 26 sections (1 dpi) (quantification in Figure 2F)
2G	n = 3 fish, 36/36 rays with fluorescence at tip
2H	n = 5 fish (0 hpi) / 8 fish (1 dpi), 12/15 rays without signal (0 hpi), 24/24 rays with signal (1 dpi)
2J-K	n = 6 fish with 8 rays (uninjured) / 7 fish with 8 rays (1 dpi), 73/73 sections without Tenascin C (uninjured), 62/72 sections with Tenascin C overlapping Zns5 at fracture + Tenascin C spreading to interrays (1 dpi)
2L-M	n = 3 fish with 7 rays with 11 sections (uninjured) / 5 fish with 9 rays with 14 sections (1 dpi), quantification in Figure 2M

3A	n = 4 fish, 14/16 rays with migration towards blastema crossing segment boundary, 8/16 rays with migration beyond amp plane into the blastema

3B	n = 5 fish, 11/16 rays with migrating cells towards fracture (conversion in adjacent segment to fracture), 21/21 rays without migration (conversion 2 segments or more apart from fracture)
3C	n = 2 fish, 2/2 rays with migrating cell towards fracture (1 dpi), see Movie S1 & Movie S2, n = 2 fish (uninjured), 2/2 rays without cell migration (uninjured), see Movie S3
3D	n = 4 fish, 16/18 rays with accumulation of GFP+ cells at fracture at 2 dpi
3E	n = 2 fish (amputation) / 5 fish (fracture), 31/36 rays with weak signal (2 dpa), 33/36 with strong signal (4 dpa), 35/36 rays with weak signal (6 dpa); 10/10 rays weak signal (2 dpi), 8/10 rays with strong signal (4 dpi), 10/10 rays with strong signal (6 dpi)
3E	n = 2 fish (amputation) / 5 fish (fracture), 33/36 rays with strong signal (3 dpa), 32/36 rays with very strong signal (4 dpa); 18/19 rays with strong signal (3 dpi), 11/19 rays with very strong signal (4 dpi)
3E	n = 2 fish (amputation) / 5 fish (fracture), 25/29 rays with expression at amp (6 dpa), 26/29 rays with expression at amp (10 dpa); 8/17 rays without expression in fractured segment (6 dpi), 9/17 rays with expression in fractured segment (6 dpi), 2/17 rays with weak expression in fractured segment (10 dpi), 15/17 rays with stronger expression in fractured segment

4B	n = 5 fish (3 dpi) / 4 fish (7 dpi) / 9 fish (uninjured - contralateral sides), 5/5 injuries with little islands of bone (3 dpi), 3/4 filled with bone matrix (7 dpi), 9/9 with intact bone (uninjured)
4C	n = 4/4 fish with distinct Calcein+ spots (3 dpi), 3/4 fish with strong Calcein signal in injury area (7 dpi), 2/2 fish with residual Calcein signal (14 dpi)
4D-E	n = 4 fish, quantification in Figure 4E
4F	n = 3 fish (7 dpi) / 3 fish (uninjured - contralateral sides) / 5 fish (14 dpi), 25/25 sections with GFP signal (uninjured), 24/25 sections without GFP in and around injury (7 dpi), 56/56 sections with GFP signal in and around injury (14 dpi), see also quantification in Figure S5
4G	n = 5/5 without GFP signal (uninjured), 5/5 fish with strong ring-shaped GFP signal at injury site (4 dpi), 4/5 fish with strong GFP signal and small hole left & 1/5 fish with strong GFP signal and bigger hole left (9 dpi), 4/5 fish with injury area covered by new bone with strong GFP signal & 1/5 fish with injury area left with small hole and strong GFP signal (14 dpi), 3/3 fish with injury area completely covered and weak GFP signal (5 wpi)
4H	n = 4 fish with 40/42 sections without GFP signal (0 hpi), n = 4 fish with 56/62 sections with GFP signal in injury area (7 dpi), n = 2 fish with 18/18 sections without GFP signal
4I	n = 4/5 fish without nuclear GFP+ cells in injury area & 1/5 with very few cells in injury area (Ethanol), 5/6 fish with nuclear GFP+ cells in injury area (4-HT)

Table S2. Experimental numbers for supplementary figures and movies

Figure	Experimental Numbers
S1A	n = 5 fish with 10 rays analyzed, 36/36 sections with epidermal thickening
S1C	n = 5 fish with 15 rays analyzed (0 hpi, 1/6/28 dpi) / 3 fish with 9 rays analyzed (13/17 wpi), 15/15 rays with fracture (0 hpi), 15/15 rays with epidermal thickening overlying fracture (1 dpi), 14/15 rays with callus, and crack visible, 15/15 rays thickened but crack not visible (28 dpi), 9/9 rays thickened (13 & 17 wpi)
S1D	n = 5 fish, 14/15 rays with fractured segments still recognizable at 1 ypi
S2A-B	n = 5 fish (*osteocalcin*:GFP) with 15 fractured and 15 uninjured fin rays analyzed (Plot profile tool ImageJ)
S2C	n = 3 fish with 7 rays with 11 sections (uninjured) / 5 fish with 9 rays with 14 sections (1 dpi), 1695 osteoblasts counted on all sections (uninjured), 2026 osteoblasts counted on all sections (1 dpi)
S2D-F	n = 3 fish with 11 rays (uninjured & 1 dpi each), uninjured: 8 necrotic osteoblasts & 21 necrotic epidermal cells in total, 1 dpi: 5 necrotic osteoblasts & 126 necrotic epidermal cells in total
Movies 1/2/3	n = 2 fish (*entpd5*:Kaede), 2/2 rays with migrating cell towards fracture (1 dpi), n = 2 fish (uninjured), 2/2 rays without cell migration (uninjured)
S3	n = 4 fish (*entpd5*:Kaede), 14/16 rays with migration towards blastema crossing segment boundary, 8/16 rays with migration beyond amp plane into the blastema
S3	n = 5 fish (*entpd5*:Kaede), 11/16 rays with migrating cells towards fracture (Kaede conversion in adjacent segment to fracture), 21/21 rays without migration (Kaede conversion 2 segments or more apart from fracture)
S4	n = 2 fish (amputation) / 5 fish (fracture, 4 for 10 dpi) (both *runx2*:GFP), 36/36 rays without signal (0 hpa, 1 dpa), 31/36 with weak signal (2 dpa), 33/36 with strong signal (4 dpa), 35/36 rays with weak signal (6 dpa), 36/36 rays with very weak signal (10 dpa); 10/10 rays without signal (0 hpi, 1 dpi, 10 dpi), 10/10 rays weak signal (2 dpi), 8/10 rays with strong signal (4 dpi), 10/10 rays with strong signal (6 dpi), 8/8 rays with weak signal (10 dpi)
S4	n = 2 fish (amputation) / 5 fish (fracture) (both *osterix*:nGFP), 36/36 rays without signal (0 hpa to 2 dpa), 33/36 rays with strong signal (3 dpa), 32/36 rays with very strong signal (4 dpa); 15/15 rays with low signal (0 hpi), 18/18 rays with low signal (1 dpi), 19/19 rays with low signal (2 dpi), 18/19 rays with strong signal (3 dpi), 11/19 rays with very strong signal (4 dpi)

S4	n = 2 fish (amputation) / 5 fish (fracture) (both *osteocalcin*:GFP), 29/29 rays with GFP in distal stump (0 hpa), 21/29 rays with reduced GFP in distal stump (1 dpa), 28/29 rays with reduced GFP in distal stump (2 dpa), 27/29 rays without expression at amp (3 dpa), 24/29 rays without expression at amp (4 dpa), 25/29 rays with expression at amp (6 dpa), 26/29 rays with expression at amp (10 dpa);15/15 rays with signal (0 hpi), 10/17 rays with reduced expression in fractured segment (1 & 2 dpi), 15/17 rays without signal in fractured segment (3 dpi), 16/17 rays without signal in fractured segment (4 dpi), 8/17 rays without expression in fractured segment (6 dpi), 9/17 rays with expression in fractured segment (6 dpi), 2/17 rays with weak expression in fractured segment (10 dpi), 15/17 rays with stronger expression in fractured segment
S5	n = 3 fish (7 dpi) / 3 fish (uninjured - contralateral sides) / 5 fish (14 dpi) (*osteocalcin*:GFP), 25/25 sections with GFP signal (uninjured), 24/25 sections without GFP in and around injury (7 dpi), 56/56 sections with GFP signal in and around injury (14 dpi), see also quantification in Figure S4